Available online at www.sciencedirect.com
SCIENCE DIRECT®
Journal of Computational Physics 201 (2004) 753–770
JOURNAL OF COMPUTATIONAL PHYSICS
www.elsevier.com/locate/jcp

Three-dimensional anisotropic mesh adaptation for phase change problems

Youssef Belhamadia, André Fortin *, Éric Chamberland

Département de mathématiques et de statistique, GIREF, Université Laval, Québec, Canada G1K 7P4

Received 7 October 2003; received in revised form 28 June 2004; accepted 28 June 2004
Available online 25 August 2004

Abstract

A three-dimensional adaptive strategy for the finite element simulation of phase change problems is presented, discussed and validated. A semi-phase-field formulation is used for the solution of the Stefan problem. The adaptive method is based on the definition of edge length using a solution dependent metric and produces strongly anisotropic meshes. Numerical results illustrating the performance and accuracy of the proposed method are presented.

Keywords: Stefan problem; Phase change; Semi-phase-field formulation; Finite element method; Error estimator; Metric; Three-dimensional anisotropic mesh adaptation

1. Introduction

The two-phase Stefan problem can be used to model phase change in various applications. The computational domain Ω is three-dimensional and consists of solid and liquid phases Ω_s and Ω_l separated by a moving interface Γ which is located on the isotherm $T = T_f$ (T_f being the melting temperature). The Stefan problem can be written as

$$\rho_i c_i \frac{\partial T}{\partial t} - \nabla \cdot (\boldsymbol{K}_i \nabla T) = f_i \quad \text{in} \quad \Omega_i, \qquad i = s, l, \tag{1}$$

where $\boldsymbol{K}_i$ is the thermal conductivity tensor (W/m K), ρ_i is the density (kg/m^3), c_i is the specific heat (J/kg K) and f_i is a possible heat source (W/m^3). At the interface Γ between the phases, the temperature T (in K) is continuous and a heat balance equilibrium condition must also be enforced on Γ which takes the form

* Corresponding author. Tel.: 418 656 3489; fax: 418 656 3404.
E-mail address: afortin@giref.ulaval.ca (A. Fortin).

0021-9991/$ - see front matter
doi:10.1016/j.jcp.2004.06.022

$$(\boldsymbol{K}_s\nabla T)\cdot\boldsymbol{n}_s+(\boldsymbol{K}_l\nabla T)\cdot\boldsymbol{n}_l=\rho_l L V_\Gamma \quad \text{on} \quad \Gamma,$$

where L is the latent heat of fusion (J/kg) and V_Γ is the interface normal velocity (m/s). This last relation is known as the Stefan condition.

Solving this problem is not an easy task, specially in the three-dimensional case. The imposition of the heat balance boundary condition impose to precisely locate the position of the interface. In Belhamadia et al. [1], a two-dimensional adaptive strategy based on the introduction of a hierarchical error estimator was used in conjunction with a so-called semi-phase-field formulation of the Stefan problem. Many two-dimensional test cases were successfully solved showing the potential of the method. It was clearly shown that anisotropic meshes are particularly efficient to determine the position of the evolving interface. It also allows to reduce substantially the number of elements necessary to obtain accurate results, both for the temperature and freezing front position. The main focus of this paper is to extend the methodology introduced in Belhamadia et al. [1] to three-dimensional problems. A different error estimator will be used which is based on the definition of edge length using a solution dependent metric as described in a series of papers by Habashi and co-workers [2–4].

The layout of this paper is as follows: in the next section the semi-phase-field model is briefly recalled. Section 3 is devoted to a description of the adaptive strategy and the numerical results are presented in Section 4. The numerical examples are three-dimensional generalizations of classical two-dimensional benchmark problems. The results clearly show the advantage of anisotropic mesh adaptation methods over classical finite element methods.

2. Semi-phase-field formulation

The semi-phase-field formulation of the Stefan problem is now briefly recalled and the reader is referred to Belhamadia et al. [1] for a complete discussion. The idea is to start from the enthalpy formulation of the Stefan problem (1) which can be written as

$$\frac{\partial H}{\partial t}-\nabla\cdot(\boldsymbol{K}\nabla T)=f, \tag{2}$$

where $\boldsymbol{K}=\boldsymbol{K}_i$, $f=f_i$ in Ω_i and the enthalpy H is defined by

$$H=\begin{cases}\rho_s c_s T & \text{in } \Omega_s,\\ \rho_l L+\rho_s c_s T_f+\rho_l c_l(T-T_f) & \text{in } \Omega_l.\end{cases}$$

The semi-phase-field formulation requires the introduction of a step function ϕ defined as

$$\phi=F(T)=\begin{cases}0 & \text{in } \Omega_s, \quad \text{i.e. for } T<T_f,\\ 1 & \text{in } \Omega_l, \quad \text{i.e. for } T>T_f.\end{cases}$$

This relation is regularized in the interval $[T_\mathrm{f}-\varepsilon, T_\mathrm{f}+\varepsilon]$, where ε is a small parameter, so that the resulting curve F_ε is differentiable as illustrated in Fig. 1. The following decomposition is then introduced:

$$H=H_1+\rho_l L\phi,$$

where H_1 is now the continuous function

$$H_1=\begin{cases}\rho_s c_s T & \text{in } \Omega_s,\\ \rho_s c_s T_f+\rho_l c_l(T-T_f) & \text{in } \Omega_l,\end{cases} \quad \text{so that} \quad \frac{\partial H_1}{\partial t}=\begin{cases}\rho_s c_s \frac{\partial T}{\partial t} & \text{in } \Omega_s,\\ \rho_l c_l \frac{\partial T}{\partial t} & \text{in } \Omega_l.\end{cases}$$

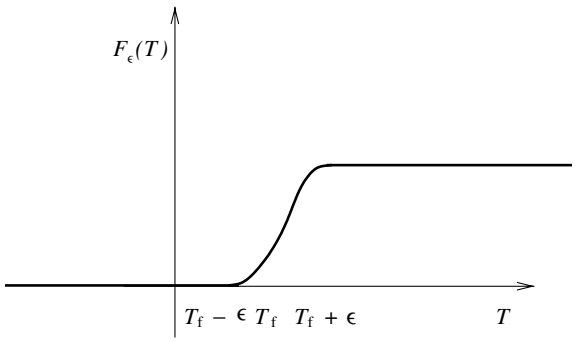

Fig. 1. Regularization of phase-field function ϕ.

Replacing in Eq. (2), a new formulation is obtained which is also equivalent to the Stefan problem. The semi-phase-field equations are then given by the regularized system

$$\begin{cases} \alpha(\phi)\frac{\partial T}{\partial t} + \rho L \frac{\partial \phi}{\partial t} - \nabla \cdot (\boldsymbol{K}(\phi)\nabla T) = f(\phi), \\ \phi = F_\varepsilon(T), \end{cases} \tag{3}$$

where:

$$\begin{cases} \alpha(\phi) = \rho_s c_s + \phi(\rho_l c_l - \rho_s c_s), \\ \boldsymbol{K}(\phi) = \boldsymbol{K}_s + \phi(\boldsymbol{K}_l - \boldsymbol{K}_s), \\ f(\phi) = f_s + \phi(f_l - f_s). \end{cases}$$

The variational formulation corresponding to system (3) is straightforward. An Euler implicit scheme is employed for the time derivatives. Starting from the solution $\phi^{(n)}$ and $T^{(n)}$ at time $t = t^n$ and multiplying the first equation by a test function v_T and the second by a test function v_ϕ, the variational formulation becomes:

$$\begin{cases} \int_\Omega \alpha(\phi^{(n+1)})\left(\frac{T^{(n+1)} - T^{(n)}}{\Delta t}\right) v_T \, \mathrm{d}\Omega + \int_\Omega \rho_l L \left(\frac{\phi^{(n+1)} - \phi^{(n)}}{\Delta t}\right) v_T \, \mathrm{d}\Omega \\ \quad + \int_\Omega \boldsymbol{K}(\phi^{(n+1)})\nabla T^{(n+1)} \cdot \nabla v_T \, \mathrm{d}\Omega = \int_\Omega f(\phi^{(n+1)}) v_T \, \mathrm{d}\Omega, \\ \int_\Omega \left(\phi^{(n+1)} - F_\varepsilon(T^{(n+1)})\right) v_\phi \, \mathrm{d}\Omega = 0. \end{cases} \tag{4}$$

Newton's method was used for the solution of the above non linear system at each time step. The linearization of system (4) is straightforward but requires the solution of huge linear systems, specially for three-dimensional applications. Direct solvers such as Gaussian elimination are not appropriate since memory requirements would rapidly exceed the capacity of available computers. Iterative methods are however more suitable but their convergence is often capricious. Fortunately, in the specific case of the system (4), a GMRES solver [5] from the PETSc library [6] preconditioned by an incomplete LU decomposition (ILU) proved to be very efficient when combined with a compressed sparse row method for the storage of the tangent matrices. The number of Newton's iterations depends on the time step Δt but in all applications, 3–6 iterations were necessary to achieve convergence with a residual norm less than 10^{-6}.

3. Brief description of the adaptive method

Adaptive remeshing methods are now widely used since it is generally admitted that they are extremely helpful in order to improve the quality and accuracy of numerical simulations. A complete review of these techniques is outside the scope of this work and the reader is referred to the pioneering work of George, Frey and co-workers (see [7–9] and the references therein). One of their major contributions is the introduction of the notion of mesh anisotropy, i.e., meshes containing elements with large aspect ratio. As shall be seen in Section 4, anisotropic meshes are particularly efficient for free surfaces problems.

In Belhamadia et al. [1], a hierarchical error estimator was used for the solution of two-dimensional phase change problems. Its extension to three-dimensional problems is in course but not yet fully implemented. A more classical approach based on the definition of edge length using a solution dependent metric will thus be used in this work. This method has been abundantly described in the literature and the reader is referred to Habashi and co-workers [2–4] and Hecht and Mohammadi [10] for a complete presentation. In the following section, a very brief description of this adaptive method will be outlined.

3.1. Error estimator based on a metric

Starting from a linear approximation u_h of a solution u, the error can be written as

$$e = u - u_h,$$

where h refers to the element length. In the one-dimensional case, it is well known from elementary numerical analysis that the maximum error on an element satisfies

$$e_{\max} = \frac{h^2}{8}\frac{\mathrm{d}^2 u}{\mathrm{d}x^2}(\xi)$$

for some ξ in the element. Following the terminology of Habashi et al. [2], the equidistribution of the error is achieved on a mesh if

$$\frac{h^2}{8}\left|\frac{\mathrm{d}^2 u}{\mathrm{d}x^2}(x_i)\right| = C \tag{5}$$

at every node x_i of the domain for some prescribed tolerance C. Such a mesh is then called optimized. To achieve this goal, second order derivatives are approximated at every node x_i of the domain and Eq. (5) determines an element length map. A new mesh satisfying as much as possible the element length map is then produced and a new solution is computed.

The same analysis is possible for two and three-dimensional problems when working on element edges. An optimized mesh must satisfy

$$\frac{l^2}{8}\left|\frac{\mathrm{d}^2 u}{\mathrm{d}\boldsymbol{v}^2}(\boldsymbol{x}_i)\right| = C,$$

where l is the length of an edge starting at node $\boldsymbol{x}_i$ and $\boldsymbol{v}$ is a unit vector tangent to that edge. The tangential derivative is defined as

$$\frac{\mathrm{d}^2 u}{\mathrm{d}\boldsymbol{v}^2}(\boldsymbol{x}_i) = \boldsymbol{v}^t A(\boldsymbol{x}_i)\boldsymbol{v},$$

where A is the Hessian matrix containing second order derivatives of the unknown solution u. The Hessian can however be reconstructed from the linear solution u_h in a least square sense using the method described in [1]. The optimized mesh must then satisfy

$$\frac{l^2}{8}\boldsymbol{v}^t A(\boldsymbol{x}_i)\boldsymbol{v} = C. \tag{6}$$

If we now consider an edge between vertices $\boldsymbol{x}_i$ and $\boldsymbol{x}_j$ of length l then the unit tangential vector $\boldsymbol{v}$ is

$$\boldsymbol{v} = \frac{\boldsymbol{x}_i - \boldsymbol{x}_j}{l}$$

and from Eq. (6), the optimized mesh must satisfy

$$(\boldsymbol{x}_j - \boldsymbol{x}_i)^t A(\boldsymbol{x}_i)(\boldsymbol{x}_j - \boldsymbol{x}_i) = C \tag{7}$$

for every edge of the mesh. Supposing now that A is positive definite, Eq. (7) defines a new (Riemannian) norm

$$\|\boldsymbol{v}\|_A = (\boldsymbol{v}^t A(\boldsymbol{P})\boldsymbol{v})^{1/2} = (A(\boldsymbol{P})\boldsymbol{v}\cdot\boldsymbol{v})^{1/2}, \tag{8}$$

linking the notion of length to the finite element error. The condition for an optimized mesh becomes

$$\|\boldsymbol{x}_i - \boldsymbol{x}_j\|_A = C \tag{9}$$

for every edge of the mesh and for some given target edge length C. The choice of the constant C is delicate and not fully mastered at this time. Too small a value will lead to a very fine mesh and to expensive (but very accurate) simulations. Consequently, the constant C is often chosen to control the number of elements. Trial and error may be needed to find the appropriate level, but once chosen, it is fixed for the duration of the time-dependent simulation.

A new mesh is then obtained from the previous one by trying to satisfy Eq. (7) on every edge. The algorithm proceeds by trying to control the error or more precisely the edge lengths by edge refinement or vertex suppression. Edge swapping together with vertex displacement are then used to smooth the mesh. This must of course be done in the respect of the geometrical boundaries of the computational domain which is perhaps the main difficulty in three-dimensional problems. Special attention must be given to the local operations on the mesh in the neighborhood of the boundary. For example, edge refinement may introduce a new node located outside the computational domain. This node has to be projected on the boundary following a technique similar to the one described in Li et al. [11].

This adaptive method based on a new metric is restricted to linear approximations since, otherwise, the error is no longer related to the Hessian matrix. In this work, a quadratic approximation of the temperature is used for the computations. This quadratic solution is thus linearly reinterpolated before proceeding to the error estimation. There is definitely a loss of information in this process. This is why the hierarchical error estimator, valid for approximations of any degree, is currently being implemented.

3.2. Quality of a tetrahedron

Anisotropic mesh adaptation can produce elongated and nearly degenerate tetrahedra if care is not taken. This is why the notion of the quality of a tetrahedron must be introduced, but taking into account the metric (8).

Let $\boldsymbol{a}_1$, $\boldsymbol{a}_2$ and $\boldsymbol{a}_3$ be three vectors issued from a vertex $\boldsymbol{P}$ and let T be the tetrahedron generated by these vectors with volume $V(T)$ as illustrated in Fig. 2. When working with the Euclidian norm, the ratio

$$\frac{V(T)}{\frac{1}{6}\|\boldsymbol{a}_1\|_2\|\boldsymbol{a}_2\|_2\|\boldsymbol{a}_3\|_2}, \tag{10}$$

measures the discrepancy between the volume of the tetrahedron and the volume of the same tetrahedron if the edges $\boldsymbol{a}_i$ were perpendicular. The maximum value of this ratio is 1 and it is a good indication of the regularity of the tetrahedron.

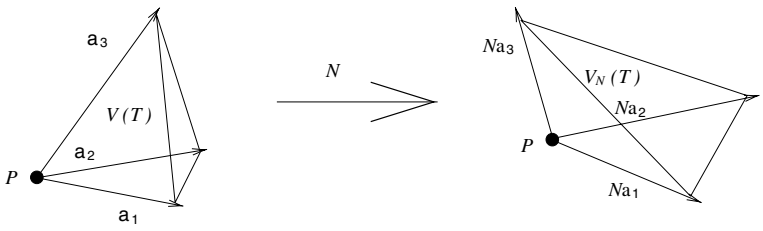

Fig. 2. Transformation of the local space.

Working with the Riemannian norm (8) not only redefines the notion of length but also that of volume. Indeed, since the Hessian matrix A is positive definite, it can be factored as

$$A = R^{\mathrm{T}} \Gamma R,$$

where R is an orthogonal matrix and Γ a diagonal matrix containing the (positive) eigenvalues of A. Setting $N = R^{\mathrm{T}} \Gamma^{1/2} R$ so that $N^{\mathrm{T}} N = A$, the length of $\boldsymbol{v}$ in the new metric becomes

$$\|\boldsymbol{v}\|_A = (N^{\mathrm{T}} N(\boldsymbol{P})\boldsymbol{v} \cdot \boldsymbol{v})^{1/2} = (N\boldsymbol{v} \cdot N\boldsymbol{v})^{1/2} = \|N\boldsymbol{v}\|_2.$$

The Riemannian norm of a vector $\boldsymbol{v}$ is the Euclidian norm of the transformed vector $N\boldsymbol{v}$. Denoting $V_N(T)$ the volume Euclidian norm of the transformed vector $N\boldsymbol{v}$

$$V_N(T) = (\det N) V(T) = (\det A)^{1/2} V(T),$$

so that the ratio (10) in the transformed space becomes

$$\frac{V_N(T)}{\frac{1}{6}\|N\boldsymbol{a}_1\|_2 \|N\boldsymbol{a}_2\|_2 \|N\boldsymbol{a}_3\|_2} = \frac{(\det A)^{1/2} V(T)}{\frac{1}{6}\|\boldsymbol{a}_1\|_A \|\boldsymbol{a}_2\|_A \|\boldsymbol{a}_3\|_A}. \tag{11}$$

Here again, this ratio measures the discrepancy between a given tetrahedron and a rectangular tetrahedron, but using the new metric.

To determine the quality of a tetrahedron, the ratio (11) is computed (and denoted Q_i) at each vertex $\boldsymbol{P}_i$ and the geometric mean is taken

$$Q(T) = \sqrt[4]{Q_1 Q_2 Q_3 Q_4}. \tag{12}$$

The quality of the elements must be as far as possible from 0 to avoid degenerate tetrahedra.

3.3. Anisotropic mesh adaptation

The objective of mesh adaptation is, starting from a solution on an initial mesh, to provide a new mesh with edge length C (see Eq. (9)) everywhere in the domain. The mesh adaptation procedure is based on a number of local operations on the initial mesh:

- edge refinement;
- edge swapping;
- vertex suppression;
- vertex displacement.

Edge refinement and vertex suppression are used in order to control edge lengths while vertex displacement and edge swapping are used to control the quality of the mesh, i.e., to avoid degenerate tetrahedra. As shall be seen, this procedure is enough to provide strongly anisotropic meshes.

In each local operation, a shell $\mathscr{S}$ is constructed consisting of elements containing the edge or vertex on which the local operation acts. This is sometimes quite difficult to obtain a convenient shell, particularly in the vicinity of the domain boundary. The algorithm then consists in sweeping the vertices and edges repeatedly and determine if a given local operation is needed:

- Edge refinement

To decide if an edge between node $\boldsymbol{x}_i$ and $\boldsymbol{x}_j$ will be halved, its length is computed using the metric of Eq. (8). This computation is performed at both extremities and averaged to give the value on the edge

$$\frac{(A(\boldsymbol{x}_i)(\boldsymbol{x}_j-\boldsymbol{x}_i)\cdot(\boldsymbol{x}_j-\boldsymbol{x}_i))^{1/2}+(A(\boldsymbol{x}_j)(\boldsymbol{x}_i-\boldsymbol{x}_j)\cdot(\boldsymbol{x}_i-\boldsymbol{x}_j))^{1/2}}{2}. \tag{13}$$

If this value is larger than the prescribed value C, the edge is halved by creating a new vertex at mid-edge. If the given edge is on the boundary, the new vertex must be projected on the geometry (CAD) of the domain.

- Vertex suppression

The edges of the mesh are swept and their length computed according to Eq. (13). If the length of an edge is too small (i.e., the error is small) then one of its vertex is removed creating a "hole" in the mesh. This "hole" is then remeshed by adding edges between some of the nodes (see Fig. 5 in [1] for the two-dimensional case). This can be done in different ways and the precise choice of the nodes to be joined is not important at this stage. The process of edge swapping (see next) will correct this choice if needed.

- Edge swapping

This operation is used to improve the quality of the elements defined in Eq. (12). The elements are first swept and their quality $Q(T)$ is computed. For a given tetrahedron, if $Q(T) < Q_{\mathrm{d}}$, where Q_{d} is a prescribed minimum value, then the edges of that element are tagged. Then all tagged edges are swept, the shell around each edge is built and the average quality of the elements in that shell is computed. Then, the shell obtained by swapping the edge is built and the average quality of the resulting new elements is computed. If the new average is larger than the initial one, the edge is swapped. Otherwise, the edge is put back in its initial position.

- Vertex displacement

A vertex can be moved inside its shell by considering that the edges form a network of springs whose stiffness is proportional to the edge error. The vertex is then moved by trying to minimize the total energy of the system. A complete description of the method and minimization technique is given in Habashi et al. [2].

Each time a new vertex is created (edge refinement) or moved, the solution u_h and its first and second order derivatives must be reinterpolated at the vertex location in order to pursue the adaptation process. If this new vertex is located in some element K, the value of u_h is computed using a fifth order Hermite polynomial as described in Belhamadia et al. [1].

The sequence of edge refinement, edge swapping, vertex suppression and vertex displacement is repeated 8–10 times. The order of the sequence can be modified at will. Experience shows that after this number of iterations, the meshes no longer evolve significantly and the edges have more or less the prescribed length C. Minimum and maximum lengths must also be added to avoid regions which are too coarse or too refined (in the vicinity of a singularity for instance).

3.4. Adaptive strategy for time dependent problems

The overall adaptive strategy is the following:

1. Starting from a solution (T^n, ϕ^n) and a mesh $\mathscr{M}^n$ at time t^n.
2. Solve system (4) on mesh $\mathscr{M}^n$ to obtain a first approximation $(\tilde{T}^{n+1}, \tilde{\phi}^{n+1})$ of the solution at time t^{n+1}.
3. Adapt the mesh on the new solution $(\tilde{T}^{n+1}, \tilde{\phi}^{n+1})$ and (T^n, ϕ^n) to obtain $\mathscr{M}^{n+1}$.

4. Reinterpolate (T^n, ϕ^n) on $\mathscr{M}^{n+1}$.
5. Solve system (4) on mesh $\mathscr{M}^{n+1}$ for (T^{n+1}, ϕ^{n+1}).

The mesh has to be adapted at each time step in order to preserve the accuracy of the solution. As described in Section 3.3, the adaptive strategy requires a linear solution u_h and the local operations on the mesh will modify the mesh in order to attain a given edge length throughout the mesh. A very simple modification of this strategy allows to take into account the variations of many scalar variables in the adaptation process. It is simply done by computing a weighted average of the different scalar functions. Determining the weight corresponding to the different functions is a delicate task and trial and error is sometimes necessary.

A crucial step is the reinterpolation of (T^n,ϕ^n) on the mesh $\mathscr{M}^{n+1}$. If care is not taken and if the new mesh is not well adapted to the solution (T^n,ϕ^n), this reinterpolation can give very poor results. This is why in step 3, we adapt the mesh on the solution $(\tilde{T}^{n+1}, \tilde{\phi}^{n+1})$ and on (T^n, ϕ^n) to avoid inaccurate reinterpolation of the solution at time t^n on the mesh $\mathscr{M}^{n+1}$. This means that the mesh is adapted on a function u which is a weighted average of $T^n, \phi^n, \tilde{T}^{n+1}$ and $\tilde{\phi}^{n+1}$.

It is also possible to adapt the mesh only on ϕ^n and $\tilde{\phi}^{n+1}$. The freezing front is then well captured but the temperature is slightly less accurate. However, the number of elements is greatly reduced since the mesh is refined only in the vicinity of the interface. In the numerical results, we will show examples will be presented where both strategies were employed.

4. Numerical results

To assess the reliability and accuracy of this numerical method and adaptive strategy, three phase change problems which are generalizations of examples treated in Belhamadia et al. [1] will be presented. In the first problem, comparisons between analytical and numerical solutions can be performed since an analytical solution exists. The last two problems are generalizations of classical two-dimensional test cases also presented in [1], Nochetto et al. [12] and Beckett et al. [13]: the formation of a cusp and the oscillating source.

As already mentioned two adaptive strategies can be used to solve these problems. Adaptation can be done taking into account both T and ϕ or by neglecting the influence of the temperature and adapting only on ϕ. Obviously, adapting on ϕ only has the major advantage of greatly reducing the number of elements since they will be concentrated only in the vicinity of the interface. Less accurate temperature prediction are however expected. Examples where both strategies were employed will be presented in the following section.

4.1. Oscillating sphere

This problem is a generalization of the two-dimensional oscillating cylinder (see [1]). Though the form of the interface is constant in this problem, it is still interesting and quite difficult. It possesses an analytical solution allowing comparisons between numerical and analytical solutions are possible.

The computational domain is the box $\Omega = [0,5] \times [-1,4] \times [-1.5,1.5]$. The interface has the form of a half-sphere of radius 1 moving up and down along the plane $x = 0$ (left-hand side in Fig. 3). Its position at all times is $(0,\alpha(t),0)$, where $\alpha(t) = 0.5 + \sin(1.25t)$. The half period of oscillation is thus $4\pi/5$.

If a proper function f is chosen (using Maple for instance), then the solution of the Stefan problem (1) is given by:

$$T(x,y,z,t) = \begin{cases} 0.75(r^2 - 1), & r < 1, \\ (1.5 - \dot{\alpha}(t)\sin\phi)(r-1), & r \geqslant 1, \end{cases} \tag{14}$$

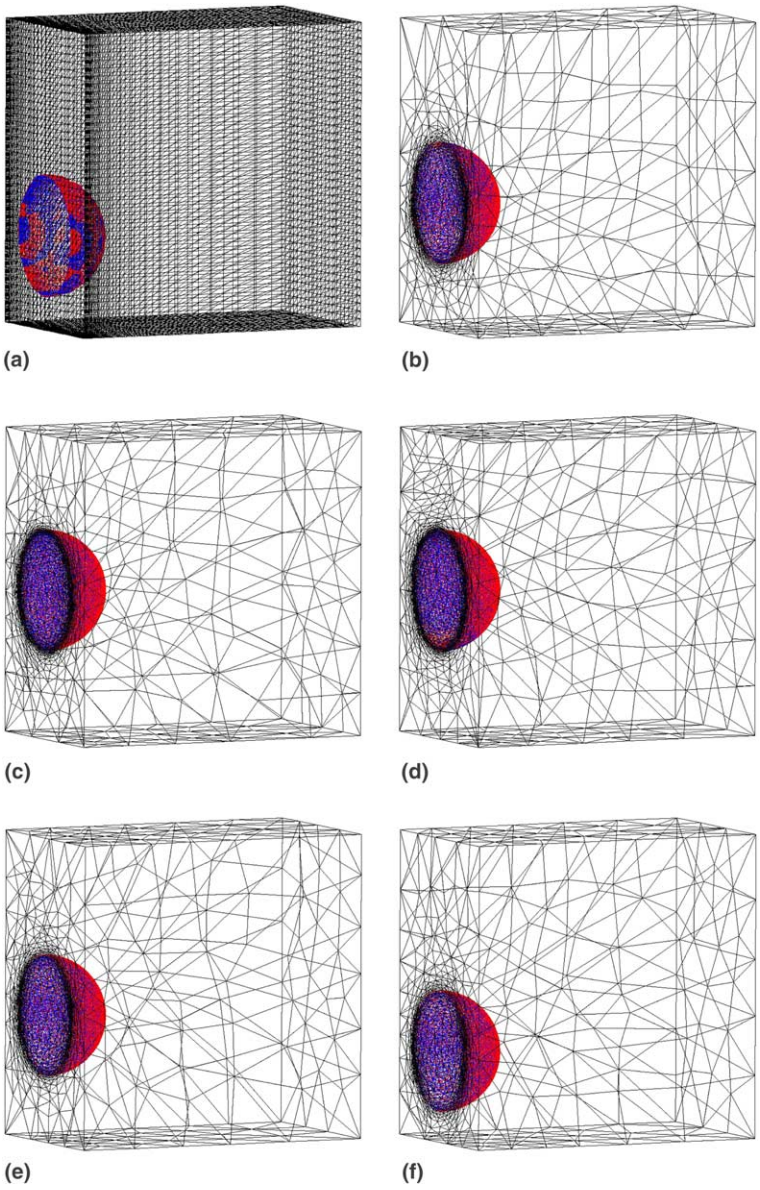

Fig. 3. *Oscillating sphere*. Time-evolution of the front over a half period: (a) $t = 0$; (b) $t = 4\pi/25$; (c) $t = 8\pi/25$; (d) $t = 12\pi/25$; (e) $t = 16\pi/25$; (f) $t = 4\pi/5$.

where $r = (x^2 + (y - \alpha(t))^2 + z^2)^{1/2}$, $\sin\phi = ((y - \alpha(t))/r)$ and $\dot{\alpha}(t) = \frac{d\alpha}{dt}(t)$. The other parameters are given in the following table:

Oscillating sphere	
$\rho_s = \rho_l = 1$	$L = 1$
$c_s = c_l = 1$	$T_f = 0$
$\boldsymbol{K}_s = \boldsymbol{K}_l = I$	

A homogeneous Neumann boundary condition is imposed on the plane $x = 0$ (where the center of the sphere is located). The initial and boundary conditions on the other sides are directly obtained from the analytical solution (14). The half period of oscillation $4\pi/5$ was divided into 100 time steps ($\Delta t = 4\pi/500$) and the regularization parameter ε was set to 0.0125.

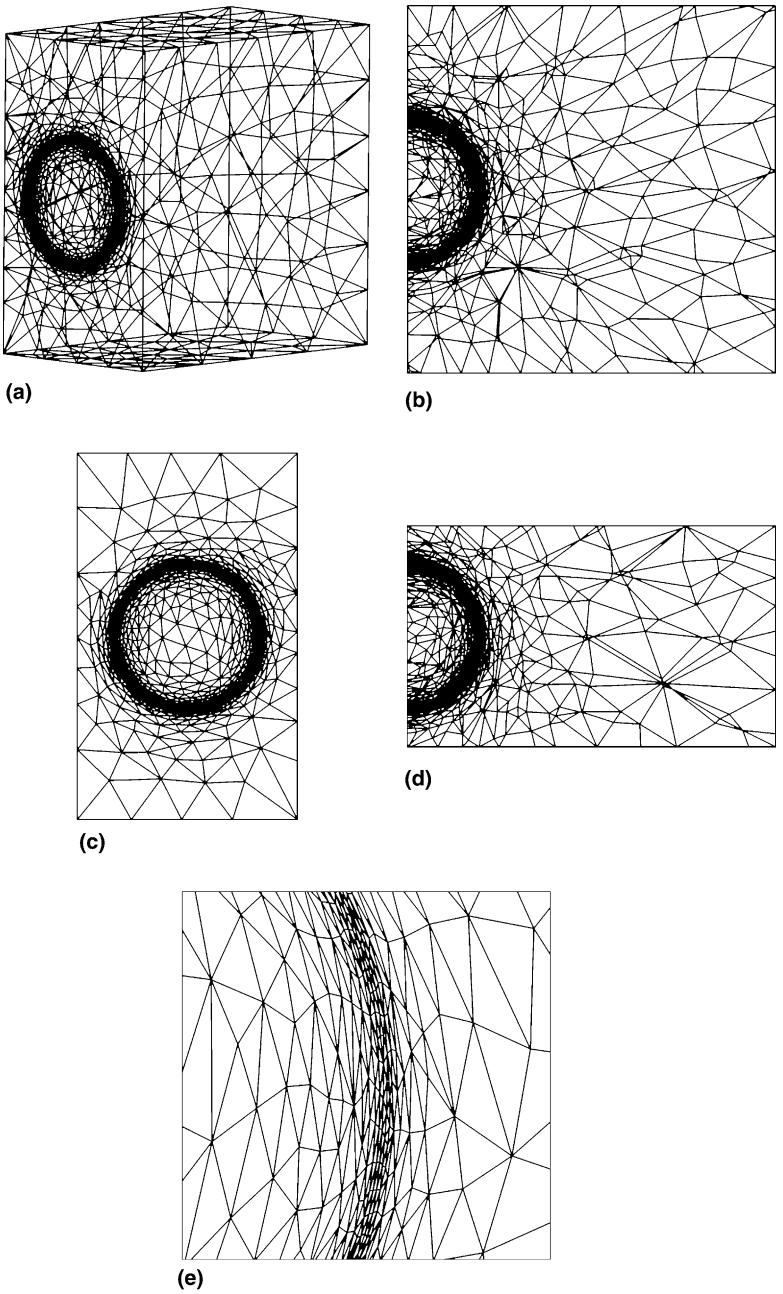

Fig. 4. *Oscillating sphere*. Cross-sections of the mesh: (a) Envelope; (b) $z = 0$; (c) $x = 0$; (d) $y = 1.5$; (e) close up view on $x = 0$.

Fig. 3 shows the interface as the sphere goes up and down the wall. The numerical solution (in blue) and the analytical one (in red) are hardly distinguishable. The initial mesh was structured ($\simeq$180,000 elements) but fortunately, at the very first time step, the number of elements is greatly reduced by the adaptive strategy. The elements are concentrated and elongated tangentially to the interface as can be clearly seen in Fig. 4 where cross-sections of the mesh in different planes passing through the sphere are presented. The last picture in Fig. 4 shows a close up view of the mesh on the interface.

4.2. Formation of a cusp

In this problem, the initial temperature condition is chosen in such a way that the solid phase takes the form of a mushroom (a cusp). This cusp starts melting, detaches from the plane $z = 0$ and then completely disappears. The two-dimensional version of this problem was considered in [1,12,13].

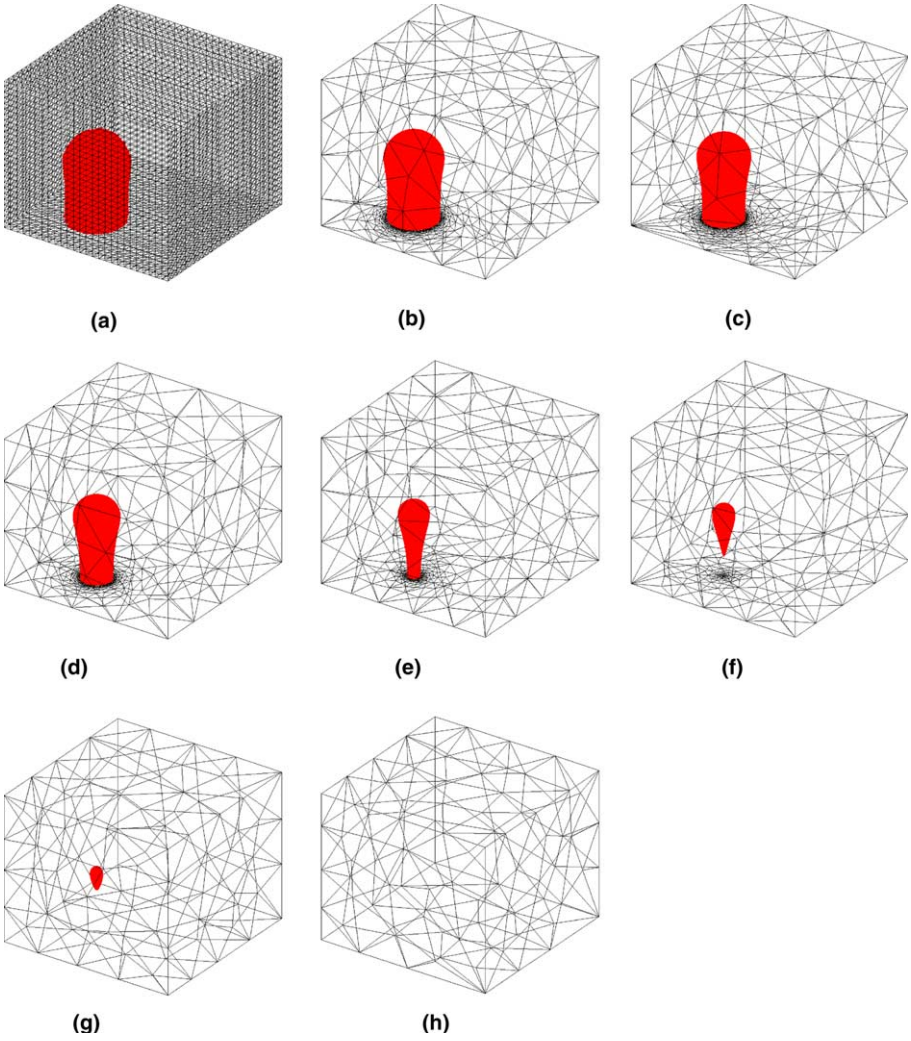

Fig. 5. *Cusp*. Isosurface $\phi = 0.5$ and mesh envelope when adapting on ϕ only: (a) $t = 0$; (b) $t = 0.0625$; (c) $t = 0.125$; (d) $t = 0.1875$; (e) $t = 0.3125$; (f) $t = 0.375$; (g) $t = 0.4375$; (h) $t = 0.5$.

The computational domain is the box $[-2,4]\times[0,5]\times[-2,4]$. The initial temperature is given by:

$$T_0(x,y,z)=\begin{cases}0.25(r^2-1) & \text{for } r\leqslant 1,\ y\geqslant 2,\\ 0.25(x^2+z^2-1) & \text{for } \sqrt{x^2+z^2}>1,\ y<1,\\ (r-1) & \text{for } r>1,\ y\geqslant 2,\\ 5(\sqrt{x^2+z^2}-1) & \text{for } \sqrt{x^2+z^2}>1,\ y<1,\\ (\sqrt{x^2+z^2}-1)(3-2\cos\pi(y-2)) & \text{for } \sqrt{x^2+z^2}>1,\ 1\leqslant y<2,\end{cases}$$

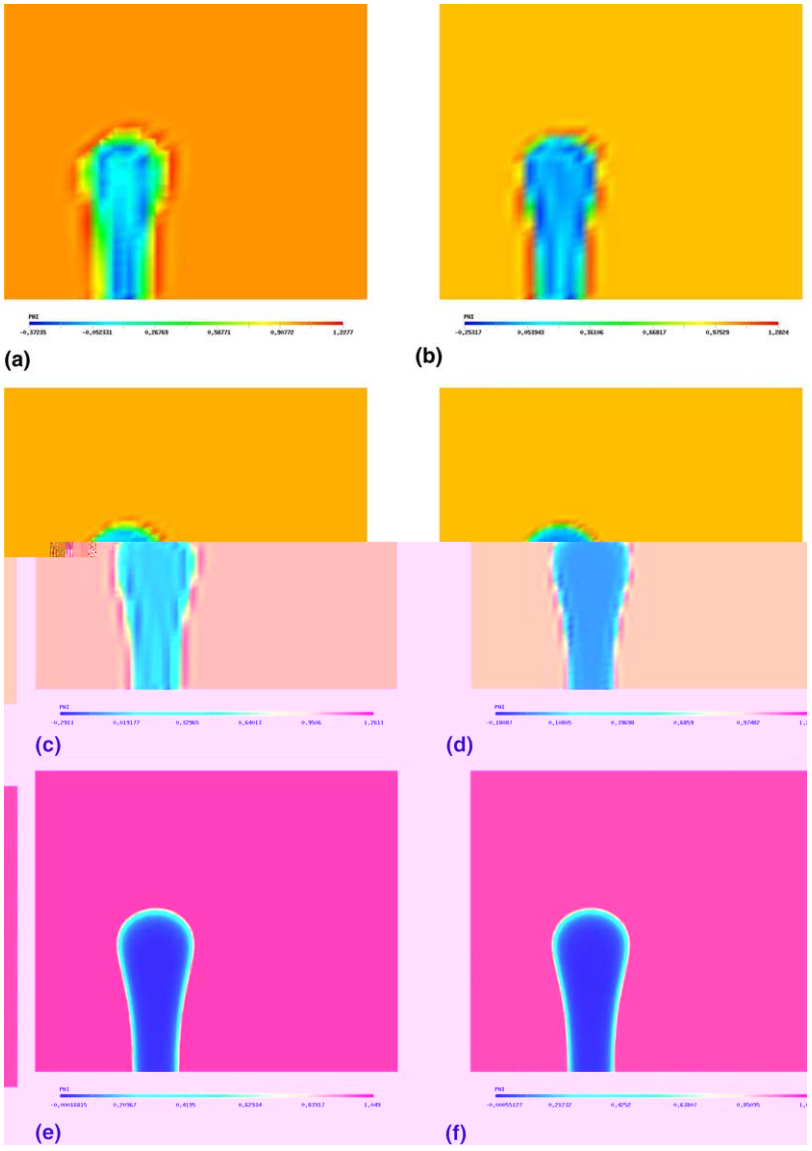

Fig. 6. *Cusp*. Cross-sections of ϕ on plane $z=0$ at $t=0.25$: (a) structured mesh, 105,456 elements; (b) structured mesh, 279,936 elements; (c) structured mesh, 584,016 elements; (d) structured mesh, 2,239,488 elements; (e) adaptation on ϕ, 28,945 elements; (f) adaptation on T and ϕ, 92,973 elements.

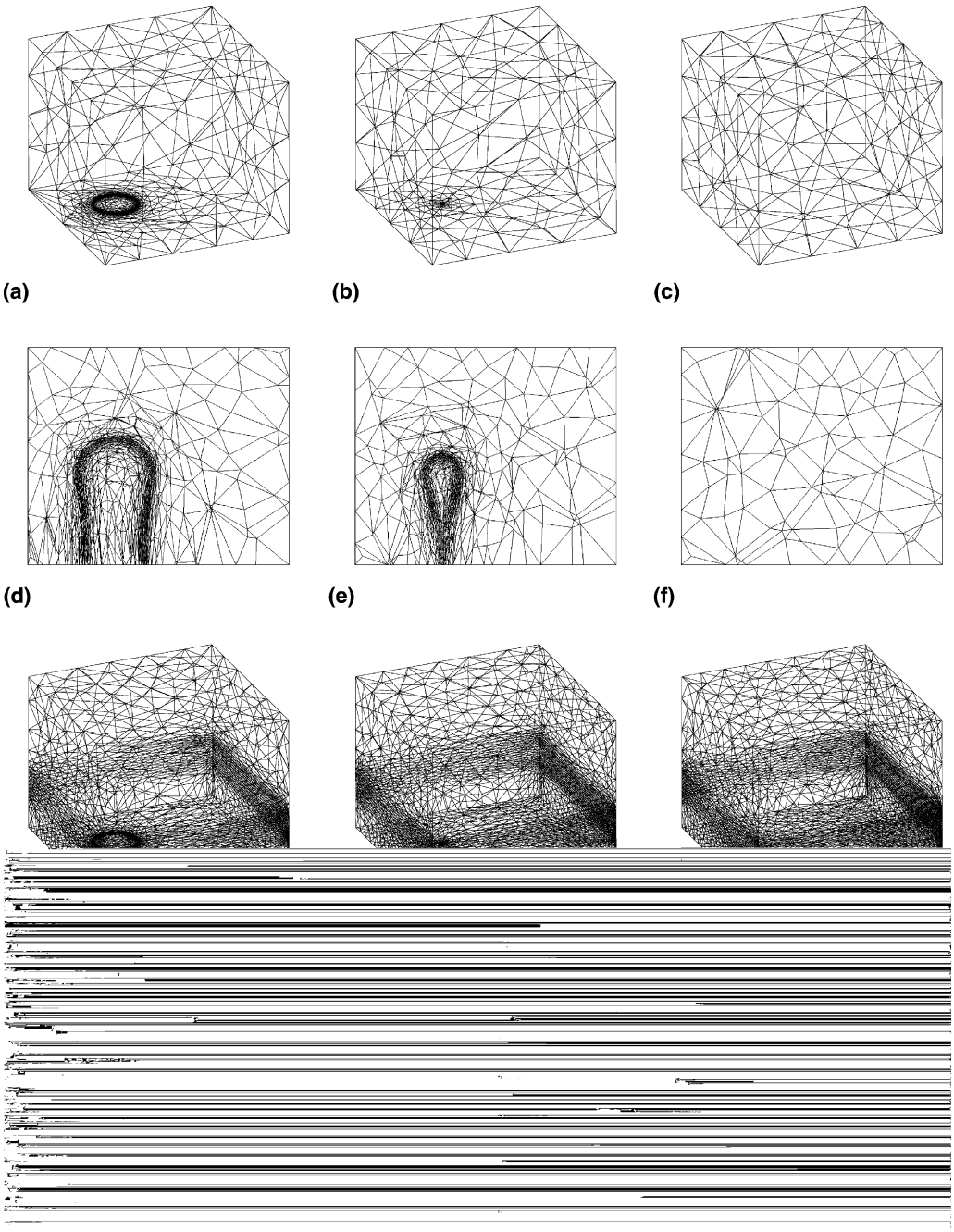

Fig. 7. *Cusp*. (a–f) Adaptation on ϕ, (g–l) adaptation on ϕ and T: (a) mesh envelope at $t = 0.125$; (b) mesh envelope at $t = 0.375$; (c) mesh envelope at $t = 0.625$; (d) mesh on $z = 0$ at $t = 0.125$; (e) mesh on $z = 0$ at $t = 0.375$; (f) mesh on $z = 0$ at $t = 0.625$; (g) mesh envelope at $t = 0.125$; (h) mesh envelope at $t = 0.375$; (i) mesh envelope at $t = 0.625$; (j) mesh on $z = 0$ at $t = 0.125$; (k) mesh on $z = 0$ at $t = 0.375$; (l) mesh on $z = 0$ at $t = 0.625$.

where $r = \sqrt{x^2 + y^2 + z^2}$. This expression is an obvious generalization of the two-dimensional version of the problem. A homogeneous Neumann condition is imposed on the side $y = 0$ and the time dependent Dirichlet boundary condition

$$T = (1 + t)T_0(x, y, z)$$

is enforced on all the other sides. The time step was set to 1/80 and the regularization parameter ε to 0.05. The other parameters are as in the oscillating sphere problem.

Initially the solid phase has the form of a cusp attached to the plane $z = 0$ and then at $t \simeq 0.33$, the interface separates from this plane and forms a closed surface. Fig. 5 presents the time evolution of the level set $\phi = 0.5$ and of the envelope of the mesh. Starting from a uniform mesh, it can be seen that the meshes easily follow the evolution of the interface. In this figure, the adaptation was performed only on the phase-field variable ϕ.

Comparisons with structured meshes clearly show the advantage of adaptive methods. Indeed, the computational domain was divided, respectively, into 105,456, 279,936, 584,016 and 2,239,488 structured elements. Fig. 6 shows cross-sections of the phase-field function ϕ on the plane $z = 0$ with the structured and adapted meshes. The adapted meshes (Fig. 6(e)–(f)) were obtained by adaptation on ϕ and on ϕ and T. As can be easily seen, the solution on the adapted meshes (with, respectively, 28 945 and 92,973 elements) are much better than even the one obtained on a structured mesh with more than 2 million elements. On the adapted meshes, the interface is very sharp and the phase-field function ϕ takes values between 0 and 1 while on the structures meshes, ϕ can take values slightly negative or larger than 1.

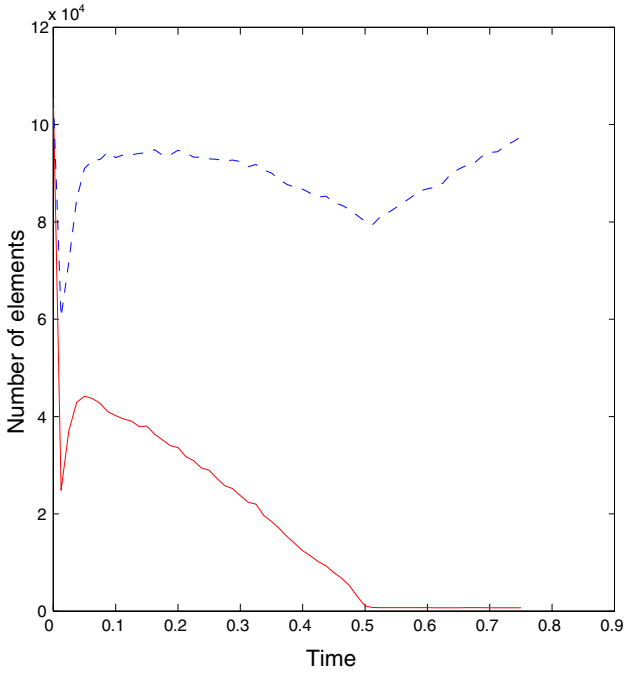

Fig. 8. Time evolution of the number of elements for both adaptation strategies: red for adaptation on ϕ and blue for adaptation on ϕ and T. (For interpretation of the references to colour in this figure legend, the reader is referred to the web version of this article.)

Finally, Fig. 7 shows a comparison of the meshes obtained when adapting on ϕ only (a–f) and on both ϕ and T (g–l). The number of elements is greatly reduced if adaptation is performed only on ϕ since the meshes are almost uniform far from the interface. This can be seen in Fig. 8, where the number of elements is presented for both strategies. Adapting on ϕ only produces meshes with a minimal number of elements when the cusp disappears (at $t \simeq 0.5$). The adaptation on ϕ and T shows however the presence of strong temperature variation coming from the boundary conditions. Clearly, adaptation on ϕ and T is more likely

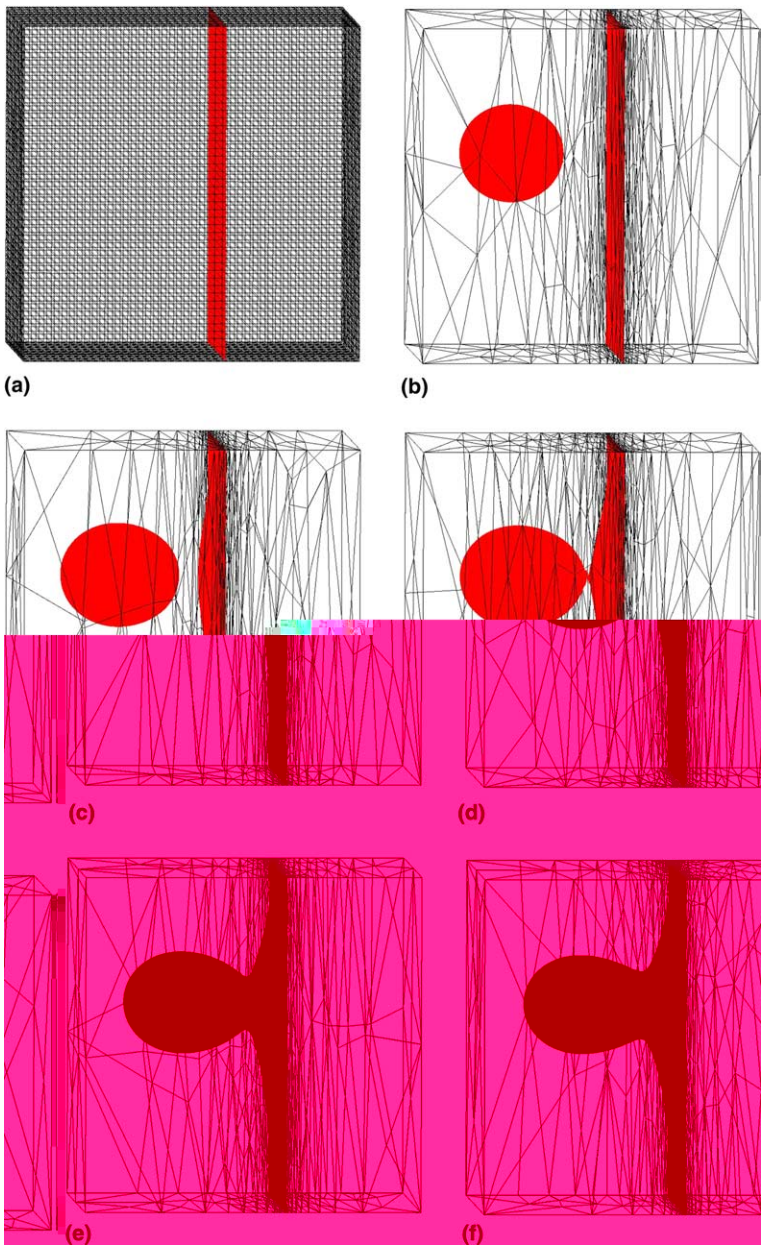

Fig. 9. *Oscillating source*. Interface and mesh envelope adapting on ϕ only: (a) $t = 0$; (b) $t = 1$; (c) $t = 2$; (d) $t = 2.5$; (e) $t = 3$; (f) $t = 3.5$.

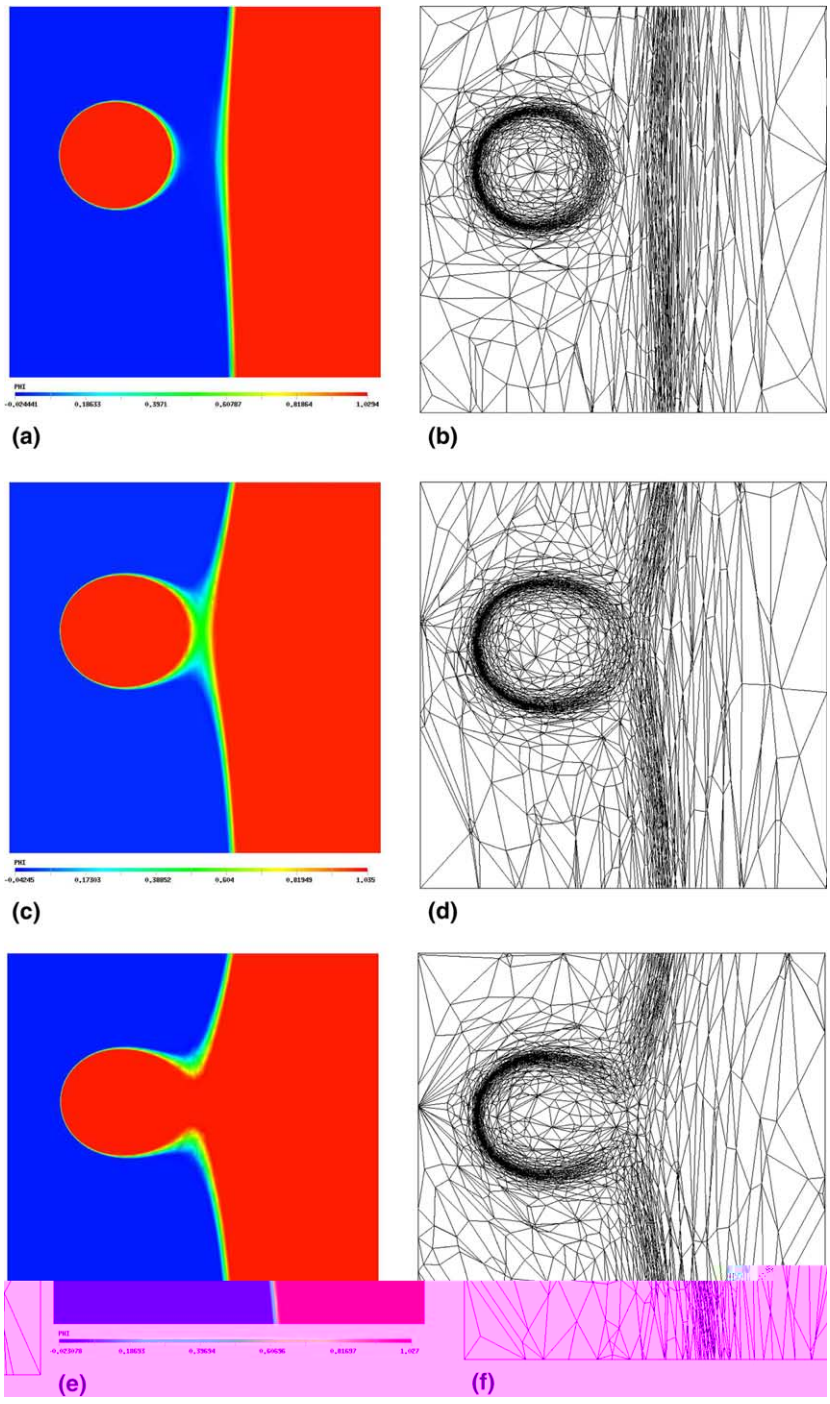

Fig. 10. *Oscillating source*. Cross-section of ϕ and of the on the plane $\Omega \cap \{z = 0\}$: (a) ϕ on plane $z = 0$ at $t = 1$; (b) mesh on plane $z = 0$ at $t = 1$; (c) ϕ on plane $z = 0$ at $t = 2.5$; (d) mesh on plane $z = 0$ at $t = 2.5$; (e) ϕ on plane $z = 0$ at $t = 3.5$; (f) mesh on plane $z = 0$ at $t = 3.5$.

to detect any important fluctuation of the temperature which could have consequences on the position of the interface. This is not the case in this problem since the interface location is the same with both strategies.

4.3. Oscillating source

In this last test case, an oscillating source problem which was also solved in two dimensions in reference Nochetto et al. [12] is considered. The computational domain is the cube $[-1,1]\times[-1,1]\times[-1,1]$. No exact solution is known for this problem. The initial temperature is given by

$$T(x,y,z) = 0.1(x-0.2)$$

and a Dirichlet boundary condition $T(x,y,z) = 0.1(x-0.2)$ is enforced on all sides. The time step was set to 0.1 and the regularization parameter ε to 0.0025. The other parameters are as in the oscillating sphere problem. The heat source f for this problem is given by

$$f(x,y,z,t) = \cos\left(\frac{t}{5}\right)\max\left(0,37-1000\left(\left(x+\frac{1}{2}\right)^2+\left(y-\frac{1}{5}\right)^2+z^2\right)\right).$$

Here again, this expression is a generalization of the two-dimensional case. The interest of this problem is that the source term is time-oscillating thus provoking strong changes in the interface position and form as illustrated in Fig. 9, where the mesh was adapted taking into account only the variations of ϕ.

Fig. 10 shows the evolution of the interface (isosurface $\phi = 0.5$) and of the mesh over time on the plane $z = 0$. Once again, the interface is very sharp and well captured.

5. Conclusions

An adaptive remeshing method based on a semi-phase-field formulation for the solution of phase change problems was presented. The adaptive remeshing strategy is based on the definition of a solution dependent metric related to the discretization error. Two adaptive strategies were used: adapting on ϕ and T or adapting on ϕ only. The presented numerical examples shows that the numerical method coupled with the adaptive strategies provides extremely accurate prediction on both the temperature and interface position for three-dimensional phase change problems.

Acknowledgement

The authors acknowledge the financial support of NSERC project SKALPEL-ITC.

References

[1] Y. Belhamadia, A. Fortin, É. Chamberland, Anisotropic mesh adaptation for the solution of the stefan problem, J. Comput. Phys. 194 (1) (2004) 233–255.

[2] W.G. Habashi, J. Dompierre, Y. Bourgault, D. Ait Ali Yahia, M. Fortin, M.-G. Vallet, Anisotropic mesh adaptation: towards user-independent, mesh-independent and solver-independent CFD. Part I: general principles, Int. J. Numer. Meth. Fluid 32 (2000) 725–744.

[3] D. Ait Ali Yahia, G. Baruzzi, W.G. Habashi, M. Fortin, J. Dompierre, M.-G. Vallet, Anisotropic mesh adaptation: towards user-independent, mesh-independent and solver-independent CFD. Part II: structured grids, Int. J. Numer. Meth. Fluid 39 (2002) 657–673.

[4] J. Dompierre, M.-G. Vallet, Y. Bourgault, M. Fortin, W.G. Habashi, Anisotropic mesh adaptation: towards user-independent, mesh-independent and solver-independent CFD. Part III: unstructured meshes, Int. J. Numer. Meth. Fluid 39 (2002) 675–702.
[5] Y. Saad, Iterative Methods for Sparse Linear Systems, PWS Publishing Company, 1996.
[6] S. Balay, K. Buschelman, V. Eijkhout, W. Gropp, D. Kaushik, M. Knepley, L.C. McInnes, B. Smith, H. Zhang, PETSc Users Manual. Technical Report ANL-95/11-Revision 2.1.6, Argonne National Laboratory, Argonne, Illinois, 2003. Available from: http://www.mcs.anl.gov/petsc/.
[7] P.J. Frey, P.L. George, Mesh Generation. Application to Finite Elements, Hermés Science Publishing, Paris, 2000.
[8] P.L. George, P.J. Frey, Non-isotropic grids, in: J.F. Thompson, B.K. Soni, N.P. Weatherill (Eds.), Handbook of Grid Generation, CRC Press, Boca Raton, FL, 1999.
[9] P.L. George, H. Borouchaki, P.J. Frey, P. Laug, E. Saltel, Mesh generation and mesh adaptivity: theory and techniques, in: E. Stein, R. de Borst, T.J.R. Hughes (Eds.), Encyclopedia of Computational Mechanics, John Wiley & Sons Ltd, New York, 2004.
[10] F. Hecht, B. Mohammadi, Mesh adaptation by metric control for multi-scale phenomena and turbulence, AIAA (1997) 97–0859.
[11] X. Li, M.S. Shephard, M.W. Beall, Accounting for curved domains in mesh adaptation, Int. J. Numer. Meth. Eng. 58 (2003) 247–276.
[12] R.H. Nochetto, A. Schmidt, C. Verdi, Adaptive solution of phase change problems over unstructured tetrahedral meshes, IMA Series (1997).
[13] G. Beckett, J.A. Mackenzie, M.L. Robertson, A moving mesh finite element method for the solution of two-dimensional stefan problems, J. Comput. Phys. 168 (2001) 500–518.